DINAME 2017 - Proceedings of the XVII International Symposium on Dynamic Problems of Mechanics
A. T. Fleury, D. A. Rade, P. R. G. Kurka (Editors), ABCM, São Sebastião, SP, Brazil, March 5-10, 2017

Rotations of the parametric pendulum excited by a reciprocating motion with a view on energy harvesting

Franco E. Dotti[1], **Florencia Reguera**[2], **Sebastián P. Machado**[1]

[1] Universidad Tecnológica Nacional, Facultad Regional Bahía Blanca, Grupo de Investigación en Multifísica Aplicada (GIMAP). Consejo Nacional de Investigaciones Científicas y Técnicas (CONICET). 11 de Abril 461, B8000LMI Bahía Blanca, Argentina. fdotti@frbb.utn.edu.ar, smachado@frbb.utn.edu.ar

[2] Universidad Nacional del Sur, Departamento de Ingeniería, Área Hidráulica. Consejo Nacional de Investigaciones Científicas y Técnicas (CONICET). Av. Alem 1253, B8000LMI Bahía Blanca, Argentina. florencia.reguera@uns.edu.ar

Abstract: In this article the nonlinear dynamics of a parametric pendulum considering a reciprocating external excitation is addressed. The interest in the study of reciprocating excitation lies in its wide use in machines and industrial equipment. The work aims at the further development of pendular devices for energy harvesting. In this context, the study is focused on the nonlinear dynamics of pendulum rotations, which are highly energetic. Although reciprocating excitation is similar to the simple sinusoidal, a different and more complex rotational behavior is observed for certain combinations of forcing and damping parameters. Among other interesting features, it is shown that a new rotation zone is present in the control space of parameters, which increases the possibilities of energy extraction.

Keywords: parametric pendulum, reciprocating motion, rotations, energy harvesting

INTRODUCTION

Based on the high kinetic energy available in its rotational motion, energy harvesting from the parametric pendulum has become a topic of growing interest for scientists and engineers (Wiercigroch, 2010; Yurchenko and Alevras, 2013; Najdecka et al., 2015; Reguera et al., 2016). The basic idea of the devices consists of a pendulum with a vertical motion induced by an energy source. If one succeeds to maintain stable rotations of the pendulum, a generator attached to the axis of rotation could be able to extract electrical energy. Although conceptually simple, the technology is still at laboratory stage mostly due to the complex nonlinear dynamics of the system. Two sources of ambient vibrations are mainly considered as external excitation: vibrating machines and the motion of the sea waves. For both cases, rotations are only possible for some forcing scenarios. But in vibrating machines, a steady harmonic forcing is present, which is much more predictable than the stochastic motion of the waves. This predictability is an important feature in the design of a suitable pendulum harvester, since it can be performed in terms of the forcing parameters, improving the ability of achieving rotations.

Since the research aims at the development of pendular devices for energy harvesting, this work is focused on rotating motion. This is because, being the parametric pendulum a problem of escape from a potential well, rotations represent the most energetic motion (Thompson and Stewart, 2003; Nandakumar et al., 2012). Reciprocating motion is taken into account as external excitation. This motion can be found in a wide range of industrial machines, including engines and pumps, where a crank-rod system is used to convert circular motion into linear motion or vice versa. Although reciprocating motion is similar to sinusoidal, which is the classical excitation in literature, it is slightly more complex (Rattan, 2009). Thus also a more complex rotational behavior of the pendulum can be expected, and this is confirmed in the results.

The article is organized as follows. After this introduction, the governing equation of the system under study is presented. The main section of the paper is devoted to the exploration of rotatory dynamics of the pendular system, including a quick overview of rotating responses, a study of the influence of the parameters and an integrity analysis of the basins of rotations. Finally, the main conclusions of the study are summarized and discussed.

THE PARAMETRIC PENDULUM EXCITED BY A RECIPROCATING MOTION

The governing differential equation of the parametrically excited pendulum of Fig. 1 can be set up by using Lagrange's equation for single-DOF non conservative systems, and its derivation can be easily followed in any classic book of nonlinear dynamics (Thompson and Stewart, 2003; Thomsen, 2003). It is a second-order ordinary differential equation given by

$$ml^2\frac{d^2\theta}{d\tau^2}+c\frac{d\theta}{d\tau}+ml\left(\frac{d^2y}{d\tau^2}+g\right)sin\,\theta=0, \tag{1}$$

where m is the mass of the pendulum bob, l the distance between the center of gravity and the pendulum axis, c the viscous damping coefficient, τ the time, g the acceleration of gravity, $y(\tau)$ the vertical displacement of the pendulum axis, and θ is the angle measured from the hanging position.

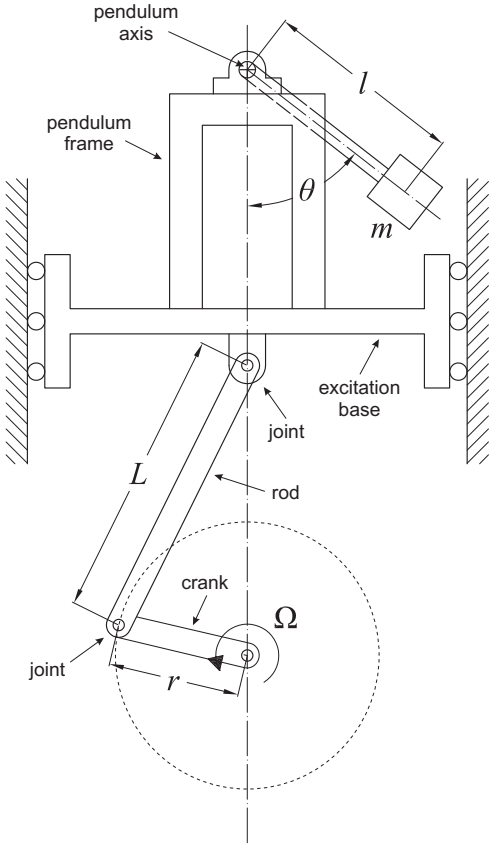

Figure 1 – The parametric pendulum, excited in vertical direction by a reciprocating motion.

A reciprocating motion provided by a crank-rod system (Rattan, 2009) constitutes the imposed motion $y(\tau)$ to the pendulum device. This is shown in Fig. 1. The connecting joint between rod and crank rotates at a constant frequency Ω, following a circumferential trajectory. Thus, the displacement of that joint projected horizontally or vertically is sinusoidal in time. However, the angle between the rod and the vertical direction is continuously changing during the cycle of motion. Therefore the linear motion of the upper end of the rod is more complex than a simple sine function. Such excitation gives to the pendulum axis the following displacement

$$y = r\left(1 - cos\,\Omega\tau\right) + L\left(1 - \sqrt{1 - \lambda^2\, sin^2\,\Omega\tau}\right), \tag{2}$$

where r is the crank radius, L is the length of the rod and the crank/rod ratio is $\lambda = r/L$. Introducing Eq. (2) into Eq. (1) the non-dimensional governing equation of the problem is obtained as

$$\ddot{\theta} + \beta\dot{\theta} + \left(R\,cos\,\omega t + \lambda^3 R\frac{\Lambda_3}{\Lambda_1^3} + \lambda R\frac{\Lambda_2}{\Lambda_1} + 1 \right) sin\,\theta = 0, \tag{3}$$

where the following definitions have been made

$$\omega_0 = \sqrt{\frac{g}{l}}, \quad t = \omega_0\tau, \quad \beta = \frac{c}{ml^2\omega_0}, \quad \omega = \frac{\Omega}{\omega_0}, \quad R = \frac{r\omega^2}{l},$$
$$\Lambda_1 = \sqrt{1 - \lambda^2\, sin^2\,\omega t}, \quad \Lambda_2 = cos^2\,\omega t - sin^2\,\omega t, \quad \Lambda_3 = cos^2\,\omega t \cdot sin^2\,\omega t. \tag{4}$$

In Eq. (3) the superimposed dot means the derivative with respect to dimensionless time t. The magnitudes R, ω and β are non-dimensional control parameters associated respectively to the forcing amplitude, forcing frequency and damping. Depending on the settings of the parameters λ, R, ω and β, and the choice of initial conditions θ_0 and $\dot{\theta}_0$, several steady state solutions of Eq. (3) can be obtained, corresponding to different responses of the physical system (Clifford and Bishop, 1995). These responses include: the rest position, oscillations, rotations and chaos.

EXPLORING ROTATING ATTRACTORS

Overview

In this section, the existence of rotating attractors for different configurations of the parametric pendulum under reciprocating excitation is explored. Eq. (3) is solved numerically by employing a dimensionless simulation time of t_s = 2500, with the purpose of ensure steady state responses. To study the rotatory dynamics of the system, control spaces, bifurcation diagrams and basins of attraction are constructed, based on extensive numerical simulations, considering different settings of the control parameters λ, R, ω and β. In the attempt to avoid transients, the first t_d = 2300 are discarded in the construction of all the diagrams.

Let's start with a quick review of rotations in a parametric pendulum. Steady state rotating solutions were first classified by Garira and Bishop (2003) in four categories: pure rotations, oscillating rotations, straddling rotations and large amplitude rotations. Among all of these solutions, pure rotations have a very significant attribute: the angular velocity always keeps the same sign ($\dot{\theta} > 0$ or $\dot{\theta} < 0$). This ensures that there is no change in the direction of rotation, implying no oscillatory motion of any kind. Pure rotations exist in conjugate pairs: clockwise and anticlockwise. A pure rotation contains high kinetic energy, being the desired motion for energy harvesting purposes. In this article, pure rotations are regarded as synonymous of *rotations*, while the other categories are considered merely as oscillations.

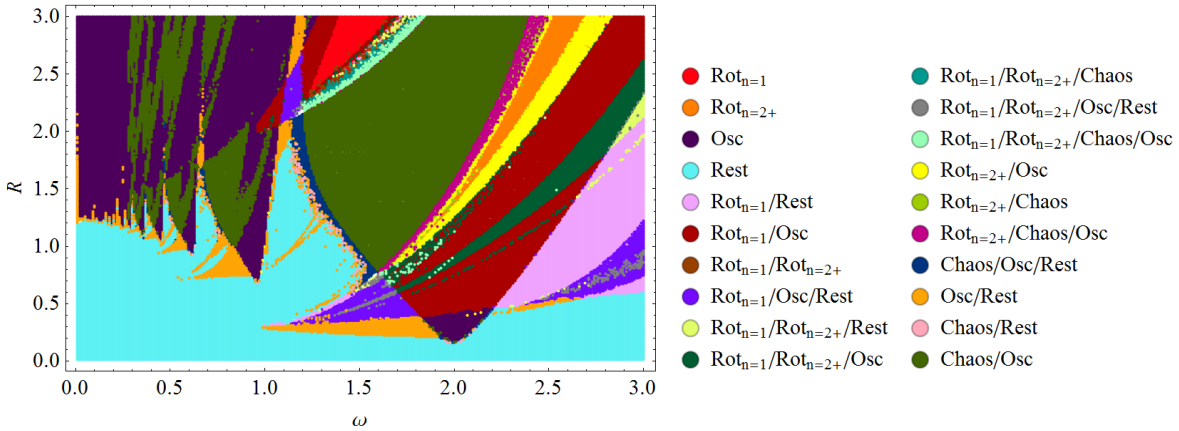

Figure 2 – Control space *R*-ω showing (approximately) all the possible physical responses of the system (λ = 0.126, β = 0.1). Rot$_{n=1}$ means "pure rotations of period 1" while Rot$_{n=2+}$ means "pure rotations of period 2 or higher". The map may have some minor inaccuracies due to the inability of the solution to escape from very long chaotic transients for some initial conditions.

For a specific set of the parameters, it is possible the coexistence of periodic and chaotic solutions, evidencing the nonlinear nature of the system. As an example, the control space R-ω of Fig. 2 (λ and β fixed) shows all the possible steady state responses. This control space is constructed as follows: for each combination of R and ω, several simulations are performed employing different initial conditions θ_0 and $\dot{\theta}_0$; then, the nature of every steady state is computed to give the color classification of the corresponding point of the graphic. It can be seen that, for low excitation amplitudes, the rest position is the commonest solution. By increasing R, oscillations, rotations and tumbling chaos appear. Although rotations are the dominant type of stable solutions in the main resonance zone (ω = 2), for most of the scenarios they coexist with other responses. Besides, there is a wide range of the control space where rotations are not possible, irrespective of the initial conditions.

Influence of the crank/rod ratio λ

The "rotation zones" of the control space R-ω are presented in Fig. 3 for different values of λ, assuming a damping of β = 0.1. Figure 3a corresponds to the classic parametric pendulum with sinusoidal forcing (actually cosinusoidal), which can be recovered from Eq. (3) by setting λ = 0. For low values of λ (say $\lambda \lesssim 0.3$), we observe in Fig. 3b-c a bifurcational behavior similar to the classic system. For higher λ (Fig. 3d), an additional rotation zone appears due to the significance of λ-terms in Eq. (3). This zone does not exist in the classic parametric pendulum for such values of R.

These additional rotating attractors are studied by means of the bifurcation diagrams of Fig. 4-5, constructed by fixing ω in the control space of Fig. 3d and plotting Poincaré points of the steady state response (a sampling time $2\pi/\omega$ is employed). In Fig. 4, up to $R \approx 1.31$, the system presents a qualitatively similar behavior to that of the classic parametric pendulum (see Dotti et al, 2015 for an equivalent bifurcation diagram with λ = 0): two period-1 symmetric rotations appear at a saddle-node bifurcation ($R \approx 0.42$), then undergo a period-doubling cascade ($R \approx 1.07$) and vanish at a crisis scenario ($R \approx 1.31$). Then, after a narrow strip of tumbling chaos, a period-6 oscillation (actually a large amplitude rotation) appears as the only stable solution for a relatively broad range of R, until it also vanishes in a crisis. At $R \approx 1.58$ tumbling chaos definitely take place. The additional rotating attractors appear at $R \approx 2.31$, maintaining as

possible solutions of the physical system up to $R = 3.5$ and above. Two minor period-3 rotating attractors are born at $R \approx 2.89$, but they soon vanish in a crisis at $R \approx 2.9$, after a rapid period-doubling cascade. Rotations and tumbling chaos coexists with the inverted pendulum solution from $R \approx 3.35$.

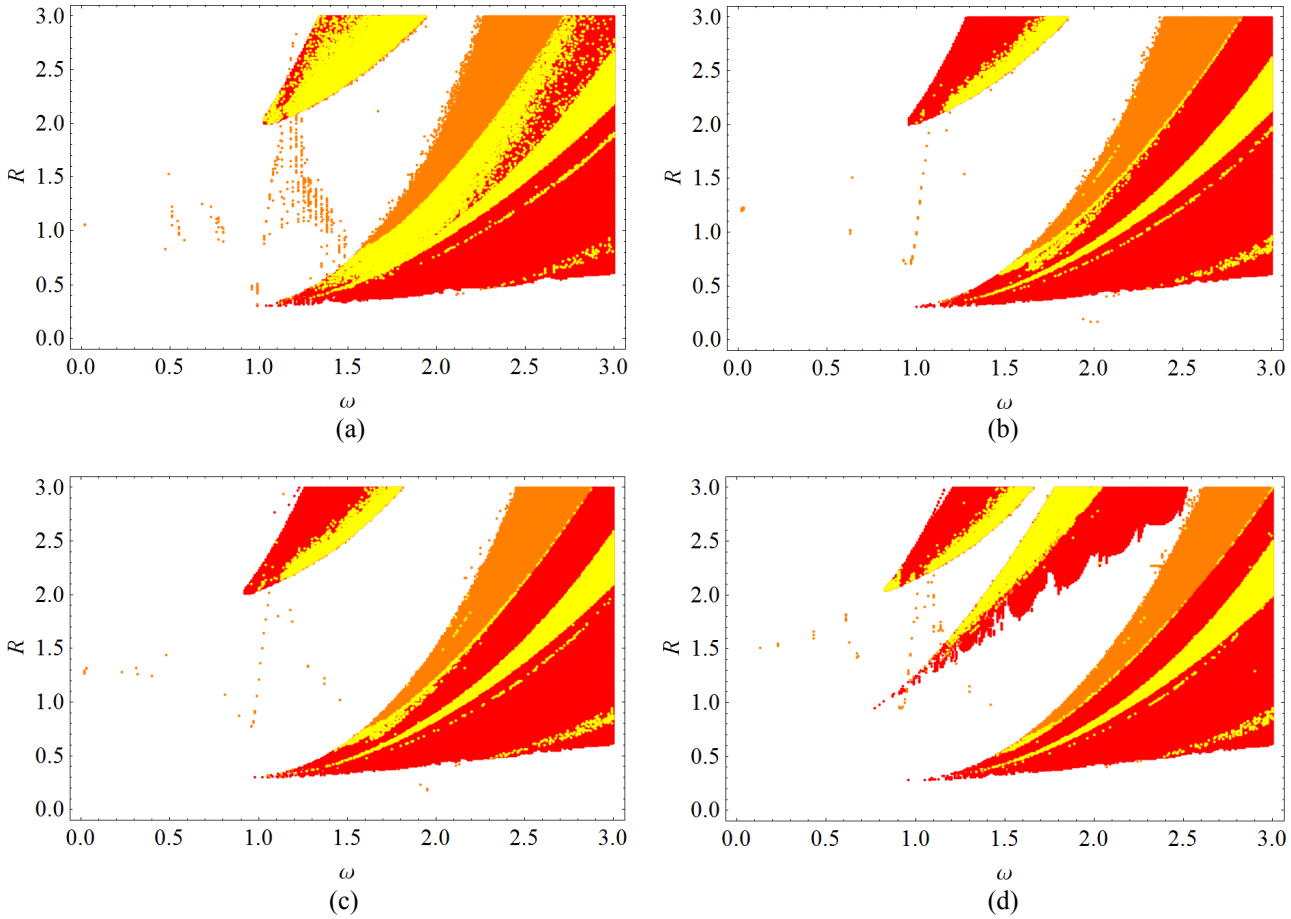

Figure 3 – Control space R-ω for the purely rotating attractors (clockwise and anticlockwise) with: (a) $\lambda = 0$, $\beta = 0.1$ (classic parametric pendulum); (b) $\lambda = 0.126$, $\beta = 0.1$; (c) $\lambda = 0.185$, $\beta = 0.1$; and (d) $\lambda = 0.356$. (•): rotations of period-1; (•): rotations of period-2 or higher; (•): coexisting period-1 and period-2 or higher rotations.

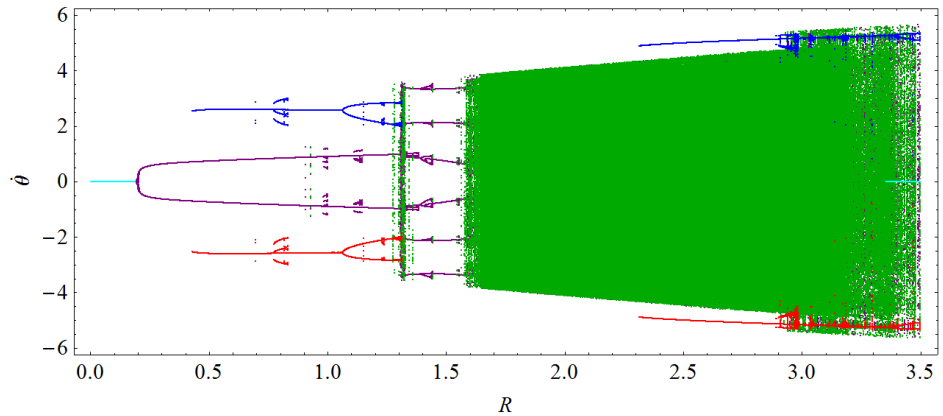

Figure 4 – Bifurcation diagram of the non-dimensional angular velocity for $\omega = 2$, $\lambda = 0.356$ and $\beta = 0.1$. (•): clockwise rotations, (•): anticlockwise rotations, (•): rest, (•): oscillations, (•): tumbling chaos.

Bifurcation diagram of Fig. 5 shows the three possible pairs of rotating attractors which can be obtained for sufficiently high values of λ. Attractors appearing at $R \approx 0.36$ and $R \approx 2.44$ exist in the classic parametric pendulum, while attractors at $R \approx 1.88$ are exclusive of the reciprocating excitation.

Figure 6 shows a bifurcation diagram of λ, obtained by fixing R, ω and β in such a way to ensure the existence of the additional rotational attractors for a high value of λ (say $\lambda = 0.356$ as in Fig 3d). As expected from Fig 3a-c, there are not stable rotating solutions for low values of λ, but as λ grows rotations appear at a saddle-node bifurcation ($\lambda \approx 0.303$). Now, being $\lambda = 0.4$ an upper practical limit of mechanical systems, results of Fig. 6 seem to indicate that an almost extreme value of λ is needed to ensure the existence of those additional rotating attractors. But the existence of

these rotating attractors is also influenced by damping, as will be explained in the next subsection.

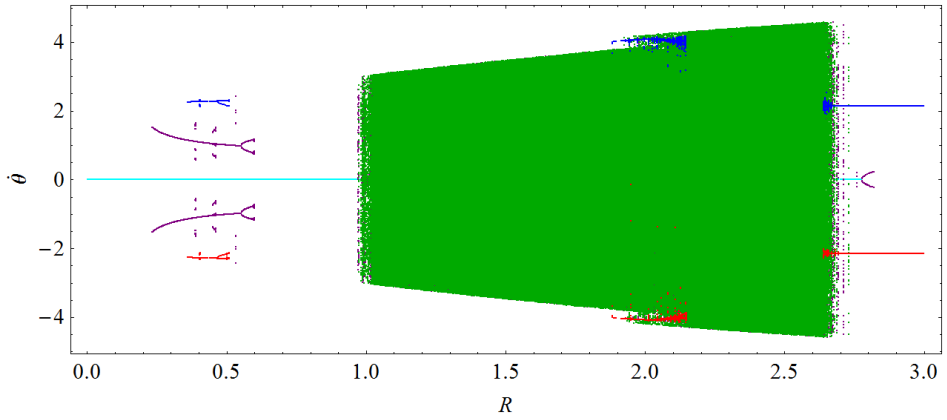

Figure 5 – Bifurcation diagram of the non-dimensional angular velocity for $\omega = 1.45$, $\lambda = 0.356$ and $\beta = 0.1$. (•): clockwise rotations, (•): anticlockwise rotations, (•): rest, (•): oscillations, (•): tumbling chaos.

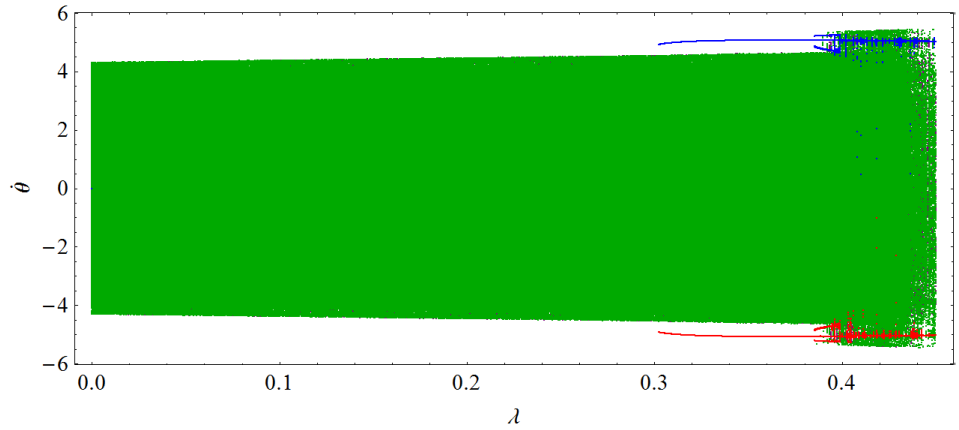

Figure 6 – Bifurcation diagram of the non-dimensional angular velocity for $R = 2.7$, $\omega = 2$ and $\beta = 0.1$. (•): clockwise rotations, (•): anticlockwise rotations, (•): oscillations, (•): tumbling chaos.

Influence of the damping parameter β

The previous study was conducted by assuming a fixed damping of $\beta = 0.1$. Besides speeding numerical integration, this value was chosen to compare the present results with many other works in literature (Clifford and Bishop, 1995; Bishop and Clifford, 1996; Thompson and Stewart, 2003; Garira and Bishop, 2003; Horton et al., 2011). But according to Nandakumar et al. (2012), damping must be of $\beta < 0.1$ in order to get a viable energy extraction. Thus, we must study what happens with a lower damping.

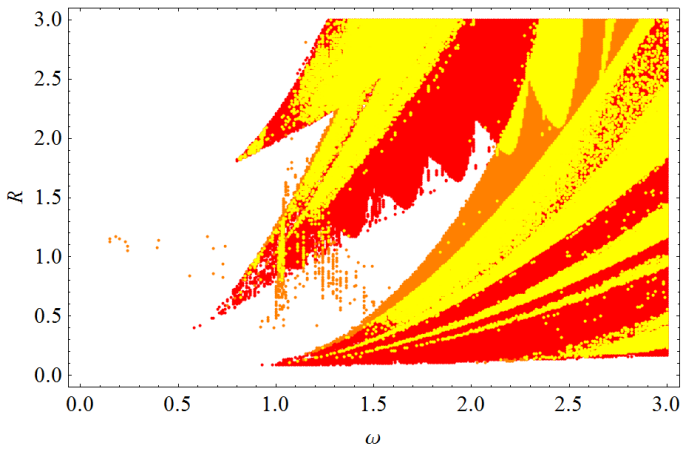

Figure 7 – Control space R-ω for the purely rotating attractors (clockwise and anticlockwise) with $\lambda = 0.126$, $\beta = 0.027$. (•): rotations of period-1; (•): rotations of period-2 or higher; (•): coexisting period-1 and period-2 or higher rotations.

For $\lambda = 0$ (simple sinusoidal excitation) it has been shown that a modification of damping moves the control space R-ω downwards or upwards, whether we decrease or increase β respectively (Leven et al, 1985; Garira and Bishop, 2003; Xu and Wiercigroch, 2007). In fact, Leven et al. (1985) pointed that an increase of the excitation amplitude (R in our system) is equivalent to a decrease of β and vice versa. A more interesting damping behavior was found for the case of a reciprocating excitation, which is evidenced by the results of Fig. 7-8. Control space of Fig. 7 can be compared with that of Fig. 3b, since for both cases $\lambda = 0.126$, with different values of β. From this comparison it is clear that, as β decreases, an additional rotation zone appears, just as happened when the parameter λ was increased (Fig. 3a-d).

As β decreases and for fixed R, ω and λ, bifurcation diagram of Fig. 8 shows the arising at $\beta \approx 0.118$ of a pair of rotational attractors at a saddle node bifurcation. This saddle node is the same presented in Fig. 6 but projected on the β-$\dot{\theta}$ plane instead of the λ-$\dot{\theta}$ of the 5D hyperspace R-ω-λ-β-$\dot{\theta}$. If a motion picture of the bifurcation diagram in Fig. 8 as λ decreases is imagined, the saddle node bifurcation would move left, until the rotating attractors completely vanish when $\lambda = 0$, leaving behind only tumbling chaos. In conclusion, with an adequate (not necessarily extremely high) value of the crank/rod ratio λ, one can ensure that the additional rotational attractors exist for a range of β where energy extraction is feasible (Nandakumar et al., 2012).

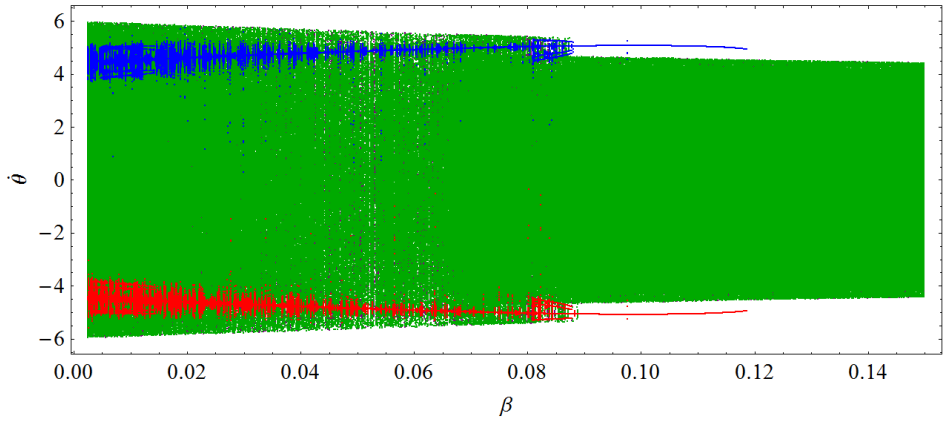

Figure 8 – Bifurcation diagram of the non-dimensional angular velocity for $R = 2.7$, $\omega = 2$ and $\lambda = 0.356$. (•): clockwise rotations, (•): anticlockwise rotations, (•): oscillations, (•): tumbling chaos.

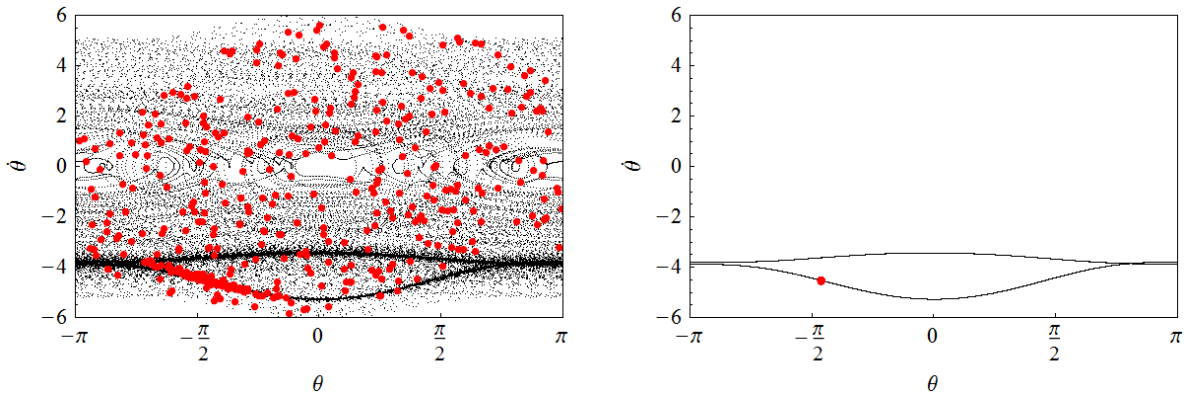

(a) (b)

Figure 9 – Phase portraits of the pendulum response and Poincaré sampling for $R = 2.7$, $\omega = 2$, $\lambda = 0.356$ and $\beta = 0.01$. Initial conditions $\theta = 2$ and $\dot{\theta} = -1.88$. Simulation time $t_s = 45000$. (a) Discarded time $t_d = 7000$, transient tumbling chaos is present. (b) Discarded time $t_d = 10000$, transient tumbling chaos is avoided and period-1 rotation is obtained. (•): pendulum response, (•): Poincaré points.

Finally, by observing Fig. 8 it follows that the period of the rotational response at low β deserves some attention. For $\beta = 0.01$, most of the rotating motions has period-1 (some of period-4 are also observed). However, steady rotations can be preceded by long periods of transient tumbling chaos (Szemplinska-Stupnicka et al., 1999). In such cases, a very long and computationally prohibitive simulation is required to avoid transient state. Figure 9 shows an example where a total of 10000 s must be discarded in order to obtain the steady period-1 rotation. This phenomenon explains the "blurred" rotating attractor of Fig. 8 and also the intermittencies in the intermediate rotation zone of the control space in Fig. 3d and Fig. 7, where only 2300 s are discarded.

Robustness and probability of rotations

After establishing the parameter settings where rotations are possible, it is very important for energy harvesting

purposes the study of the basins of attraction associated to the rotatory attractors. Basically, it is necessary to know how difficult it is to achieve a steady rotational motion, and how predictable could be this motion.

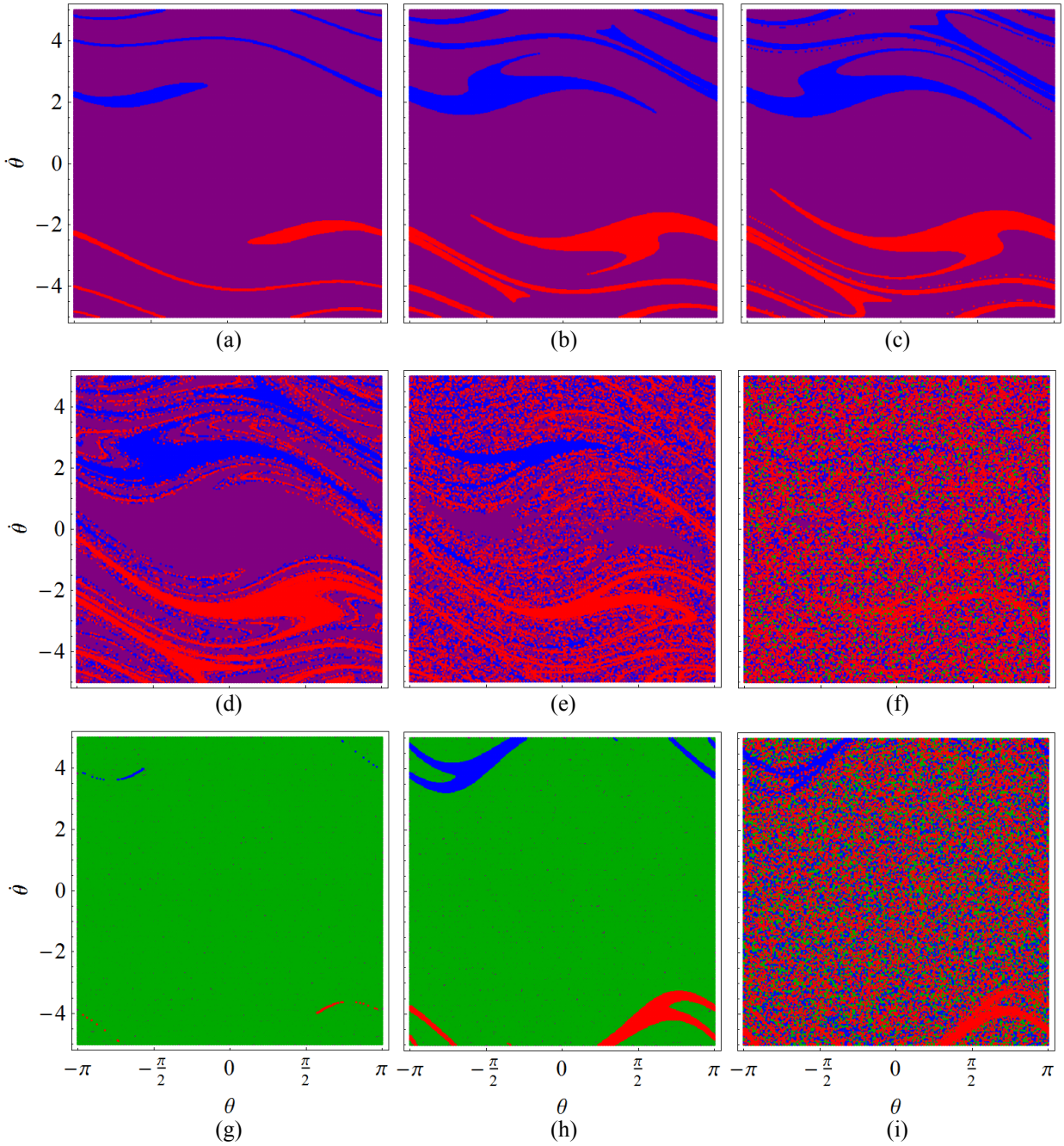

Figure 10 – Basins of attraction sequence for $\omega = 2$, $\lambda = 0.356$ and $\beta = 0.1$ as the forcing magnitude R is increased; (a) $R = 0.45$, a pair of symmetrical period-1 rotating attractors have just born; (b) $R = 0.6$, the basin of rotations grow into the basin of oscillations; (c) $R = 0.65$, a homoclinic tangency has occur and fractal erosion of the oscillatory attractor starts; (d) $R = 0.750$, fractal erosion of the oscillatory attractor progresses; (e) $R = 1$, oscillatory attractor has almost been fully eroded; (f) $R = 1.3$, basins of oscillations and rotations are both almost indistinguishable due to fractal erosion; (g) $R = 2.22$, a pair of new rotating attractors born by a saddle node; (h) $R = 2.7$, the basin of rotations grows into the basin of tumbling chaos; (i) $R = 3$, erosion of the basin of rotations is in process while the basin of tumbling chaos is fully eroded. (•): clockwise rotations, (•): anticlockwise rotations, (•): oscillations, (•): tumbling chaos.

Thus, the dynamics of the basins of rotation as R increases is followed. Figure 10 shows basins of attraction associated to the bifurcation diagram of Fig. 4, since for both graphics it is $\omega = 2$, $\lambda = 0.356$ and $\beta = 0.1$. The basins are constructed numerically by using a grid in the $(\theta_0, \dot{\theta}_0)$ starting space. There the birth of rotations at a saddle node bifurcation ($R \approx 0.425$) is observed and, as R increases, the basin of rotations grows into the basin of oscillations (Fig. 10a-b). After the homoclinic tangency (Capecchi, 1995), the basin boundary initiates its fractalization, and "fractal fingers" sweep across the basin of oscillations, leading to a progressive erosion of the entire basin (Fig. 10c-e). At R = 1.3 (Fig. 10f) the basin of rotations is almost fully eroded; there is a high *final state sensitivity*: minute variations of the

initial conditions may change the attractor ultimately chosen (Thompson and Stewart, 2003); rotating chaos is present (Leven et al., 1984; Bishop and Clifford, 1996), but it is about to be replaced by tumbling chaos. At $R \approx 1.32$ a crisis happens and then, for a broad range of R, tumbling chaos is the only stable attractor. At $R \approx 2.22$ a new basin of rotations appear "out the chaos" (Fig. 10g). This basin evolves inside the chaotic basin, until it also fractalizes from $R \approx 2.75$ on. At $R = 3$, both the basin of rotations and tumbling chaos are eroded. Rotations are of period-1 and they have long chaotic transients, as discussed in the previous subsection.

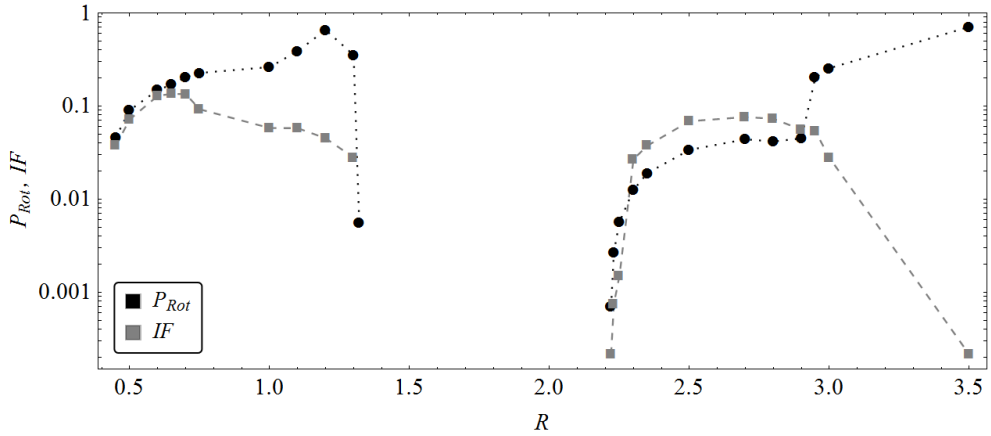

Figure 11 – Integrity and probabilistic analysis of rotations as R is increased, for $\omega = 2$, $\lambda = 0.356$ and $\beta = 0.1$.

A visual inspection of the basins of attraction such as that in Fig. 10 allows qualitative observations on the structural stability of the basins and the interaction among attractors. But with a view on energy harvesting, a quantitative evaluation of the robustness of the basins of rotations is required. For this purpose, the *integrity factor* (*IF*) is considered, which is defined in 2D cases as the normalized radius of the largest circle entirely belonging to a basin (Lenci and Rega, 2011). As rotations are studied regardless of its period, the *IF* can be thought as a measure of sensitivity of the rotating motion to initial conditions: with a high *IF* ($IF \longrightarrow 1$), a small variation of the initial conditions also produces a steady rotation; meanwhile, with a low *IF* ($IF \longrightarrow 0$), the opposite happens.

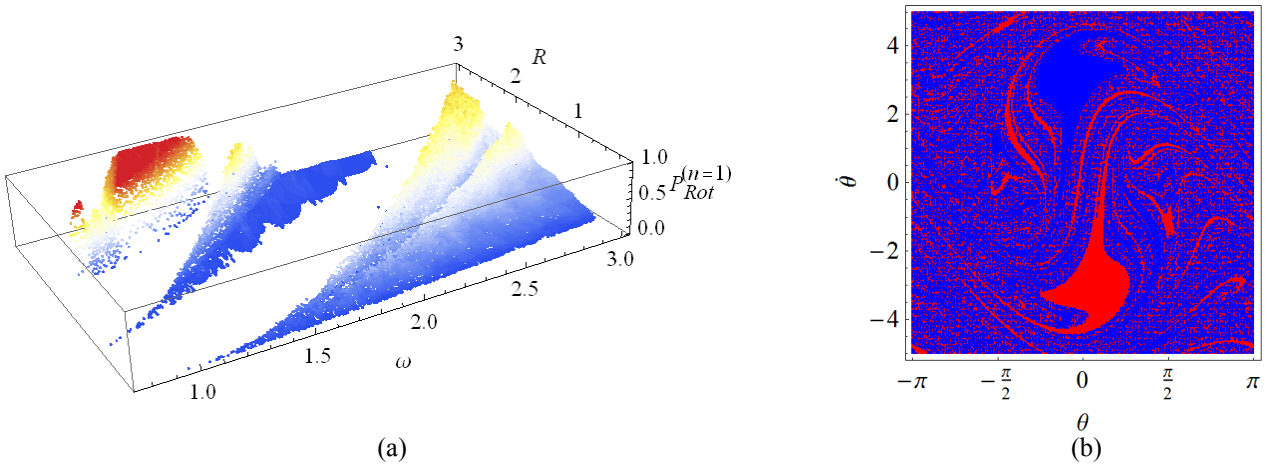

Figure 12 – (a) Probability of obtaining a period-1 rotation as steady state of the system, given random initial conditions inside the ranges $-\pi \le \theta \le \pi$ and $-5 \le \dot{\theta} \le 5$. (b) Basin of attraction for $R = 2.7$, $\omega = 1.2$, $\lambda = 0.356$ and $\beta = 0.1$; for this combination of the parameters period-1 rotations are obtained regardless of the initial conditions.

Besides, since initial conditions usually cannot be accurately determined in practice, it is important to know what happens given an unknown starting condition. Thus we define P_{Rot} as the probability of occurrence of rotations, for random initial conditions into a given range. P_{Rot} quantifies the difficulty of obtaining *any* rotation, regardless of direction and period. Being *IF* and P_{Rot} two normalized magnitudes, a comparison between them can be made.

The results of the robustness/probabilistic analysis are presented at Fig. 11. From the birth of rotations up to the beginning of the fractalization ($R \approx 0.65$, see also Fig. 10c), P_{Rot} and *IF* measures give similar increasing values since rotations are confined only into their basin. The peak of robustness is approximately at $R = 0.6$, corresponding to $IF = 0.129$. As erosion evolves, the *IF* decays because the basin of rotations loose robustness (the final state sensitivity increases), but P_{Rot} keeps increasing because more initial conditions produce rotations (see also Fig. 10d-e). At $R = 1.2$ the basin of oscillations is almost fully eroded, with a maximum number of initial conditions producing rotations ($P_{Rot} = 0.66$). At $R = 1.3$ the oscillatory basin is even smaller but thus P_{Rot} diminishes because some initial conditions produce

tumbling chaos; the basin of rotations is also very small, being *IF* close to zero (*IF* = 0.028). At this point, there is not possible in practice to predict the direction of rotations. At the crisis of $R \approx 1.32$, only a few initial conditions produce rotations: *IF* = 0 and $P_{Rot} \approx 0$. A similar behavior is observed for the pair of rotational attractors born at $R \approx 2.22$: P_{Rot} and *IF* measures give similar increasing values until erosion starts, then *IF* decays and P_{Rot} keeps growing up to a crisis, which produces in this case after $R = 3.5$. In practical terms, these attractors are robust only after $R \approx 2.4$, but rotations can be obtained for a wide range of *R*. The peak probability is $P_{Rot} = 0.71$ at $R = 3.5$, meaning that 71 % of the initial conditions produce rotations. Being $IF \approx 0$, the direction of these rotations is unpredictable.

It is interesting to note that for some settings of the parameters it could be $P_{Rot} = 1$. This means that all the initial conditions produce rotations. Actually, Fig. 12a has a "red zone" where all the responses are rotational with period-1, which is the most energetic rotating motion. Phase portrait of Fig. 12b is an example of this behavior. Due to the erosion of the basin, final state sensitivity is high; but the choice is reduced to both rotatory attractors (clockwise and anticlockwise), thus only direction of motion is unpredictable.

Note on the solutions of Figure 3

Perhaps the reader is wondering about the orange dots in odd places in Fig. 3. They represent some chaotic solutions which are wrongly indicated as high periodic rotational solutions. For a sinusoidal forcing ($\lambda = 0$), Clifford and Bishop (1995) already explained this phenomenon: some parts of a chaotic time history may appear to be periodic over a limited number of periods when the chaotic trajectory is close to an unstable solution. For example, this behavior can be observed by comparing Fig. 3b with its associated stability diagram of Fig. 13. This misplaced orange dots appear over an area close to the limits of the resonance zones, where the rest solutions turns to be unstable and an oscillating attractor is born by a Hopf bifurcation (Szemplinska-Stupnicka et al., 1999).

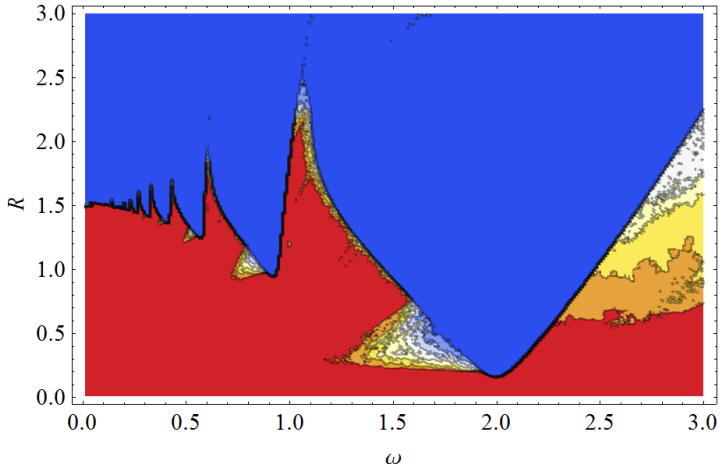

Figure 13 – Stability diagram showing the resonance zones, represented as the blue "tongues". Inside these zones the rest solution is unstable. The graphic was constructed numerically and represents a density plot of the occurrence of the rest solution ($\lambda = 0.356$, $\beta = 0.1$). Blue denotes zero, indicating that the rest position cannot be a steady response of the physical system.

CONCLUSIONS

This article aims to contribute to the development of pendulum systems for energy extraction from vibrating machines and ocean waves. The dynamics of the vertical parametric pendulum with a reciprocating external excitation was addressed. By means of nonlinear dynamics tools, a rich dynamic behavior is elucidated, with substantial differences with respect to the classic parametric pendulum with a sinusoidal excitation. Crank/rod ratio and viscous damping are found to be crucial for the rotational dynamics of the system: with a sufficiently high crank/rod ratio and/or a sufficiently low damping, new rotating attractors appear which are impossible with a sinusoidal excitation. These rotations were proven to exist for ranges of damping where energy extraction is feasible, which is very significant in terms of energy harvesting since it means that more combinations of the excitation parameters allow rotational motion, increasing the possibilities for energy extraction.

The structural stability of the rotatory attractors and the probabilities of obtaining rotations with random starting conditions were studied. It was shown that robustness and probability of rotations grow similarly until fractalization of the phase portrait starts. After this event, robustness decays due to the erosion of the basins of rotations, but probability keeps growing because increasingly initial conditions produce rotations. This situation means that rotations are easy to obtain but direction of rotation is difficult to predict due to the high final state sensitivity. The first is good for energy harvesting purposes, while the second should not lead to great difficulties in practical applications: rotations are good, regardless of their direction.

A main conclusion of this work is that with a correct configuration of non-dimensional excitation and damping

parameters, steady rotations can be easily reached and predicted. These parameters are closely related to an adequate design of the pendulum harvester, which does not represent a serious problem if the excitation is known, as commonly happens in industry. In addition, for some specific combinations of the parameters, all the realistic initial conditions produce the most energetic rotating motion: a period-1 rotation. This is very interesting for energy harvesting because, theoretically, no external control action would be needed to reach rotating motion.

Energy harvesting by means of pendulum rotations is a very attractive idea because high amounts of energy could be recovered with simple and relatively small devices. The present work contributes to the knowledge on the field, but it is only a step aiming to understand the dynamics of the mechanical system in a simplified way. Even at the laboratory stage further research is needed, which must include: active control of rotations to cope with variations of external forcing, optimization of the harvester devices for a maximum energy extraction, development of a suitable generator for the conversion of kinetic to electric energy, influence of the proper generator dynamics, influence of the synchronization phenomenon in multi-pendular systems, and several others. Thus, many challenges must be faced until this could be a viable, practical, and commonly implemented technology. But given the global need for clean energy, these challenges are likely to be addressed in the near future.

ACKNOWLEDGMENTS

The authors thank the support of Secretary of Science and Technology and Secretary of International Relations of Universidad Tecnológica Nacional, CONICET and Engineering Department of Universidad Nacional del Sur.

REFERENCES

Bishop, S.R. and Clifford, M.J., 1996, Zones of chaotic behavior in the parametrically excited pendulum, Journal of Sound and Vibration, Vol. 189, No. 1, pp. 142-147.

Capecchi, D., 1995, Geometric aspects of the parametrically driven pendulum, Nonlinear Dynamics, Vol. 7, pp. 231-247.

Clifford, M.J. and Bishop, S.R., 1995, Rotating periodic orbits of the parametrically excited pendulum, Physics Letters A, Vol. 201, pp. 191-196.

Dotti, F.E., Reguera, F. and Machado, S.P., 2015, A review on the nonlinear dynamics of pendulum systems for energy harvesting from ocean waves, Proceedings of the 1st Pan-American Congress on Computational Mechanics – PANACM 2015, Buenos Aires, Argentina, pp. 1516-1529.

Garira, W. and Bishop, S.R., 2003, Rotating solutions of the parametrically excited pendulum, Journal of Sound and Vibration, Vol. 263, pp. 233-239.

Horton, B., Sieber, J., Thompson, J.M. and Wiercigroch, M., 2011, Dynamics of the nearly parametric pendulum, Internationa Journal of Non-Linear Mechanics, Vol. 46, 436-442.

Lenci, S. and Rega, G., 2011, Experimental versus theoretical robustness of rotating solutions in a parametrically excited pendulum: A dynamical integrity perspective, Physica D, Vol. 240, pp. 814-824.

Leven, R.W., Pompe, B., Wilke, C. and Koch, B.P., 1985, Experiments on periodic and chaotic motions of a parametrically forced pendulum, Physica D, Vol. 16, pp. 371-384.

Najdecka, A; Narayanan, S. and Wiercigroch, M., 2015, Rotary motion of the parametric and planar pendulum under stochastic wave excitation, International Journal of Nonlinear Mechanics, Vol. 71, pp 30-38.

Nandakumar, K., Wiercigroch, M. and Chatterjee, A., 2012, Optimum energy extraction from rotational motion in a parametrically excited pendulum, Mechanics Research Communications, Vol. 43, pp.7-14.

Rattan, S.S., 2009, Theory of machines, Ed. Tata McGraw Hill, New Delhi, 705 p.

Reguera, F., Dotti, F.E. and Machado, S.P., 2016, Rotation control of a parametrically excited pendulum by adjusting its length, Mechanics Research Communications, Vol. 72, pp. 74-80.

Szemplinska-Stupnicka, W., Tyrkiel, E. and Zubrzycki, A., 2000, The global bifurcations that lead to transient tumbling chaos in a parametrically driven pendulum, International Journal of Bifurcation and Chaos, Vol. 10, No. 9

Thompson, J.M. and Stewart, H.B., 2003, Nonlinear dynamics and chaos, Ed. John Wiley & Sons, West Sussex, England, 437 p.

Thomsen, J.J., 2003, Vibrations and stability, Ed. Springer-Verlag, Berlin, Germany, 420 p.

Wiercigroch, M., 2010, A new concept of energy extraction from waves via parametric pendulor. UK Patent Application.

Xu, X. and Wiercigroch, M., 2007, Approximate analytical solutions for oscillatory and rotational motion of a parametric pendulum, Nonlinear Dynamics, Vol. 47, pp. 311-320.

Yurchenko, D. and Alevras, P., 2013, Dynamics of the N-pendulum and its application to a wave energy converter concept. International Journal of Dynamics and Control, Vol. 1, No. 4, pp. 290-299.

RESPONSIBILITY NOTICE

The authors are the only responsible for the material included in this paper.